Isolated cavities dominate Greenland Ice Sheet dynamic response to lake drainage.

Jessica Mejia[1], Jason Gulley[1], Celia Trunz[2], Matthew David Covington[3], Timothy Bartholomaus[4], Surui Xie[1], and Timothy H Dixon[1]

[1]University of South Florida
[2]University of Arkansas
[3]University of Arkansas at Fayetteville
[4]University of Texas at Austin

November 23, 2022

Abstract

Seasonal variability in the Greenland Ice Sheet's (GrIS) sliding speed is regulated by the response of the subglacial drainage system to meltwater inputs. However, the importance of channelization relative to the dewatering of isolated cavities in controlling seasonal ice deceleration remains unsolved. Using ice velocity, moulin hydraulic head, and glaciohydraulic tremor measurements we show the passing of a subglacial floodwave following the drainage of an up-glacier supraglacial lake slowed minimum sliding speeds to wintertime background values without increasing the hydraulic capacity of the moulin-connected drainage system. We interpret these results to reflect a persistent basal traction increase consistent with the dewatering of isolated cavities exert the dominant control on seasonal ice velocity decreases. Current predictions of the GrIS's ice-dynamic response to increased surface melting hinges on the subglacial drainage system's ability to increase its capacity to offset sustained meltwater influxes, which our results demonstrate may not be the case.

Isolated cavities dominate Greenland Ice Sheet dynamic response to lake drainage.

J. Z. Mejia[1], J. D. Gulley[1], C. Trunz[2], M. D. Covington[2], T. C. Bartholomaus[3], S. Xie[4], T. Dixon[1]

[1]Department of Geosciences, University of South Florida, 4202 E. Fowler Ave. Tampa, FL 33620.
[2]Department of Geosciences, University of Arkansas, 1 University of Arkansas, Fayetteville, AR 72701
[3]Department of Geological Sciences, University of Idaho, 875 Perimeter Drive, Moscow, ID 83844
[4]Scripps Institution of Oceanography, University of California San Diego, 9500 Gilman Drive, MC 0225, La Jolla, CA 92093

Key Points:

- Isolated cavity drainage governs Greenland Ice Sheet slowdowns, not increased drainage system efficiency.
- Floodwaters from rapid supraglacial lake drainages induce widespread slowdowns by dewatering isolated cavities.
- Ice sliding speeds may be more sensitive to persistent meltwater inputs than previously thought.

Corresponding author: Jessica Mejia, jessicamejia@usf.edu

Abstract

Seasonal variability in the Greenland Ice Sheet's (GrIS) sliding speed is regulated by the response of the subglacial drainage system to meltwater inputs. However, the importance of channelization relative to the dewatering of isolated cavities in controlling seasonal ice deceleration remains unsolved. Using ice velocity, moulin hydraulic head, and glaciohydraulic tremor measurements we show the passing of a subglacial floodwave following the drainage of an up-glacier supraglacial lake slowed minimum sliding speeds to wintertime background values without increasing the hydraulic capacity of the moulin-connected drainage system. We interpret these results to reflect a persistent basal traction increase consistent with the dewatering of isolated cavities exert the dominant control on seasonal ice velocity decreases. Current predictions of the GrIS's ice-dynamic response to increased surface melting hinges on the subglacial drainage system's ability to increase its capacity to offset sustained meltwater influxes, which our results demonstrate may not be the case.

Plain Language Summary

Meltwater produced on the surface of the Greenland Ice Sheet reaches the bed by flowing into crevasses or moulins, vertical conduits that reach the base of the ice sheet. Early in the summer, meltwater that reaches the bed increases water pressures within the drainage system underneath the ice sheet and increasing sliding speeds. However, later in the summer, ice sliding speeds often slowdown despite continued meltwater inputs. While these slowdowns have been attributed to the growth of channels that connect to moulins, recent observations suggest the drainage of hydraulically isolated cavities, pockets of water that form on the lee-side of bedrock bumps, may instead be responsible. Here we use measurements ice velocity and water pressures within moulins several kilometers away from rapidly draining supraglacial lakes to show that the passing of the floodwave underneath the ice-sheet slowed sliding to winter-time speeds without enlarging subglacial channels. Instead, our results indicate that the drainage of isolated cavities is responsible for slowdowns that occur during the melt season. Because the growth of subglacial channels was thought to be able to compensate for increased melting, our results suggest the Greenland Ice Sheet's ice-dynamic contribution to sea level rise may be significantly underestimated.

1 Introduction

Predicting the Greenland Ice Sheet's (GrIS) response to future climate warming scenarios is limited by gaps in understanding links between ice sheet hydrology and dynamics. Using better-studied alpine glaciers as GrIS analogs, the subglacial drainage system's hydraulic capacity is considered the primary control on sliding speeds. Ice accelerates when water inputs exceed the drainage system's hydraulic capacity, causing water to back-up englacially, which increases the pressure head at the bed and reduces basal traction (Bartholomew et al., 2012; Bartholomaus et al., 2007). Ice velocity decreases during the melt season have been interpreted to reflect a transition from an inefficient, distributed drainage system consisting of high-pressure linked cavities and till aquifers to an efficient drainage system consisting of low-pressure conduits (Sundal et al., 2011; Sole et al., 2013; Chandler et al., 2013; Colgan et al., 2011). Conduits are thought to be able to enlarge in order to accommodate sustained meltwater influxes and drain water from the surrounding inefficient drainage system, thereby reducing subglacial water pressures and slowing sliding speeds. Under this paradigm, the GrIS ice-dynamic response to future warming should be buffered by conduit enlargement.

Recent observations have shown that weakly connected, and hydrologically isolated cavities can drive seasonal decreases in ice velocity that have been widely attributed to increased drainage system efficiency. The isolated drainage system consists of water-filled cavities which form on the lee side of bedrock bumps where sliding decouples ice from the bed (Lliboutry, 1968; Walder, 1986; Iken & Truffer, 1997). Isolated cavities exist between, and are isolated from, distributed and channelized regions of the subglacial drainage system, similar to how oxbow or thermokarst lakes and ponds are disconnected from nearby rivers and streams in surficial hydrological systems. Distributed and channelized parts of the drainage system modulate pressures within isolated cavities indirectly through the transfer of mechanical support (Murray & Clarke, 1995; Meierbachtol et al., 2016), or through sliding-driven fluctuations cavity volume(Iken & Truffer, 1997). Because pressures within isolated cavities are high, these small changes in cavity volume cause water pressures to fluctuate about ice overburden pressure, modifying basal traction and modulating sliding where they are distributed over large areas of the bed (Andrews et al., 2014; Hoffman et al., 2016; Iken & Truffer, 1997; Meierbachtol et al., 2016).

Isolated cavities can connect and drain into the distributed drainage system when large influxes of water overwhelm the subglacial drainage system. Rapid basal sliding or hydraulic jacking of the ice can create transient connections between isolated cavities and nearby parts of the distributed drainage system. If isolated cavities are at higher pressure, water in them will drain into the distributed system until connections subsequently close-off when water pressures are low (Iken & Truffer, 1997; Stone & Clarke, 1996; Rada & Schoof, 2018). Consequently, isolated cavities that maintained high average subglacial water pressure and promoted sliding before the connection would have lower water pressures and therefore slowing sliding speeds. If drainage of isolated cavities is responsible for observed slowdowns (Andrews et al., 2014; Hoffman et al., 2016; Ryser et al., 2014; Hoffman et al., 2011), and not increased channelization, it is less clear how the GrIS will respond to future warming.

2 Study Site and Data

2.1 Study Area

Here we report how relationships between subglacial water pressure and ice sliding speeds changed when rapidly draining supraglacial lakes triggered a subglacial floodwave that passed beneath our study site on the GrIS. Using those changes, we infer that the dewatering of isolated cavities, not increased channelization, is responsible for seasonal decreases in ice velocity. We established a camp in the ablation area of Sermeq Avannarleq on the western GrIS (Fig. 1; 65.6°N, 49.7°W), more than 7 km downglacier from several supraglacial lakes that drained in previous years (Morriss et al., 2013; Williamson et al., 2017). Theoretical subglacial hydraulic potential gradients, which may provide information about subglacial flow paths connecting discrete inputs to downglacier areas (Gulley et al., 2012), indicated our camp was located along the theoretical subglacial flow path draining these lakes (Figure 1). On 10 July 2018, we instrumented PIRA moulin with a pressure transducer to measure water pressure in the most connected subglacial drainage system (Andrews et al., 2014). We measured ice motion using three Global Navigation Satellite System (GNSS) stations spanning approximately 750 m in the across-flow direction from GNSS station JEME, positioned near our instrumented moulin. In May 2018, we installed a seismic station near PIRA moulin to measure seismic glaciohydraulic tremor, a proxy for the subglacial flux of water within the most-connected regions of the subglacial drainage system (Bartholomaus et al., 2015), and the occurrence of icequakes associated with nearby ice fracture (Roeoesli et al., 2016). Finally, we use meteorological data from LOWC weather station (Mejia, Trunz, Covington, & Gulley, 2020), installed at our field site, filling in data gaps with data from the GC-NET (Steffen et al., 1996) weather station JAR1.

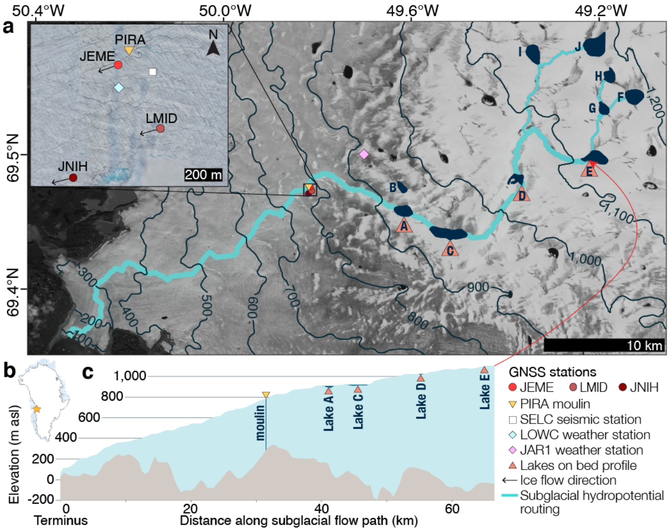

Figure 1. Study area in the Paakitsoq region of the Greenland Ice Sheet. a, Landsat-8 image (21 July 2018) of Sermeq Avannarleq with a July 2018 drone orthophoto shown in the study area zoom-in window. Site symbols are shown in the key. 100-m ice-surface elevation contours derived from BedMachine v3 (Morlighem et al., 2017) data. Maximum supraglacial lake extent filled in navy. b, Sermeq Avannarleq (yellow star) location. c, Surface and bed elevations along subglacial flow path extending from lake E to the terminus in cyan (Schwanghart & Kuhn, 2010)

2.2 Moulin Instrumentation

We instrumented moulins during the 2017 (JEME moulin, Supplementary Materials) and 2018 (PIRA moulin) melt seasons after the snowline had retreated past the site. In both years the upper 30 m of the moulins were visible and appeared vertical. We measured water pressures within each moulin using Geokon 4500HD-7.5MPa piezometers affixed to armored cable. Moulins were instrumented by lowering measured lengths of cable until the sensor reading increased with water depth, indicating we reached the water column within the moulin shaft. We then continued lowering the sensor while confirming depth increases. Upon encountering features where feeding more cable into the moulin did not change the sensor's recorded depth, we anchored the cable to the ice surface. We fixed the sensor in place within PIRA moulin at 154.5 m below the ice surface. We recorded water pressures every 15-minutes by Campbell Scientific CR-1000 data loggers equipped with AVW200 modules. We estimate an error of 20 m in our absolute moulin head measurements, arising from the uncertainty in the sensor elevation as described in detail by Andrews et al. (2014). Importantly, error in absolute moulin head does not apply to our measurements of relative change (e.g. diurnal variations) which should have an associated error on the order of centimeters.

2.3 Ice Motion and Uplift

We determined kinematic site positions from our GNSS stations (JEME, LMID, and JNIH) using TRACK software (Herring et al., 2010; Xie et al., 2019) which uses carrier-phase differential processing relative to bedrock mounted base stations. We use both GNSS stations KAGA (28 km baseline length) and ROCK (36 km baseline) as reference stations. We estimate kinematic positions using 30-second intervals that match our receiver sampling rates, we apply a 10-degree cutoff angle to reduce multi-path and use long baseline mode during processing. To minimize smoothing gaps at the boundaries of our daily

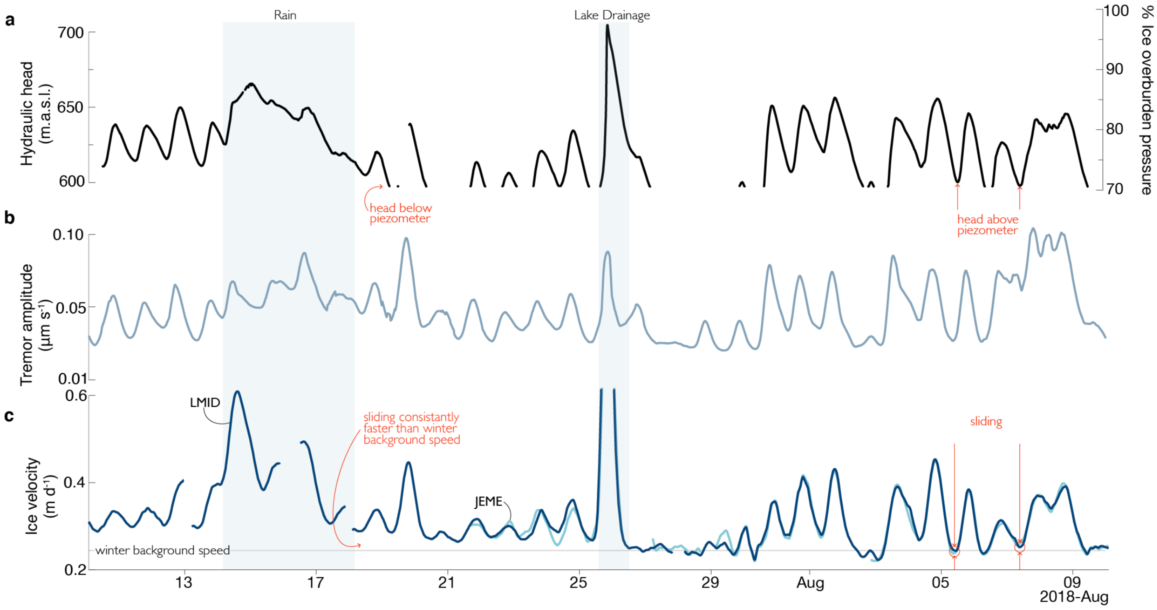

Figure 2. 2018 moulin hydraulic head, tremor amplitude, and ice velocity. a, PIRA moulin hydraulic head and as a percentage of ice overburden pressure. b, 6-h averaged glaciohydraulic tremor amplitude recorded at station SELC. c, 6-h averaged along-flow ice velocity of stations LMID (blue) and JEME (light blue). The timeseries is truncated to an upper limit of 0.6 m d^{-1} to preserve diurnal velocity minima. The full range of ice velocity (extending to 1.5 m d^{-1}) is shown in Figure 3. Gray line shows winter background speed at station LMID is 0.24 m d^{-1}. Shading in all panels corresponds to periods of heavy rainfall and the lake drainage event.

observation files, we extend each observation file with 12-hours from the surrounding days. Overlapping time periods are removed from the final position time series. The velocity and uplift calculations (Howat et al., 2008; Virtanen et al., 2020) are described in the Supplement to this paper.

2.4 Glaciohydraulic tremor and icequake record

We deployed a seismic station approximately 150 meters away from PIRA moulin in April 2018 to record local icequakes and seismic glaciohydraulic tremor amplitude, a proxy for the flux of subglacial discharge (Bartholomaus et al., 2015). This station was equipped with a Nanometrics Centaur digitizer connected to a Nanometrics Trillium Compact Posthole sensor re-installed on 12 July 2018, 1.1 m below the ice surface. We poured sand over the top of the seismometer at the time of installation to improve coupling between the sensor and surrounding ice. Ablation measurements from late July 2018 indicate that the sensor remained at least 0.5 m below the ice surface at the time supraglacial lake floodwaters passed beneath the sensor.

3 Results

Before the lake drainages in late July 2018, daily meltwater production induced clear diurnal variations in moulin hydraulic head, glaciohydraulic tremor amplitude, and ice velocity (Figure 2). Moulin hydraulic head was moderately variable, with minimum values falling below the piezometer elevation of 597 m.a.s.l. (below 73±12% of ice overburden pressure), and maximum values up to 666 m.a.s.l. (about 88±9% of overburden).

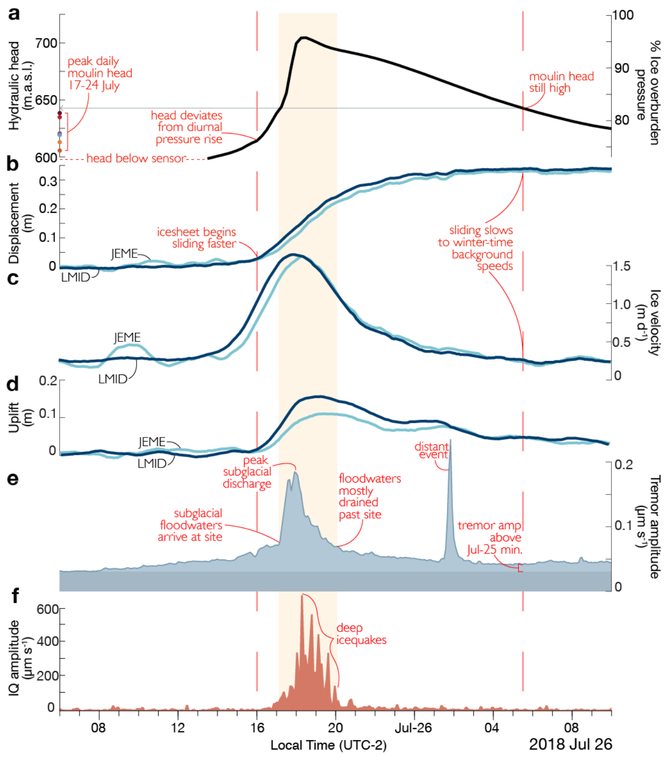

Figure 3. Coupled hydraulic, ice-dynamic, and seismic observations following the 2018 lake drainage event. a, PIRA moulin hydraulic head. b-d, GNSS station recordings from stations LMID (blue) and JEME (light blue). b, 30-minute filtered along-flow ice displacement detrended with respect to winter background motion. c, 2-h averaged along-flow ice velocity. d. 2-h averaged uplift from beginning of event. e, Glaciohydraulic tremor amplitude from seismic station SELC. f, Maximum icequake amplitude over 5-min time intervals. Red dashed lines mark the boundaries of the ice-dynamic response. Yellow shading marks when tremor amplitude suggests floodwaters were directly under our site.

Diurnal peaks in moulin water level and ice velocity were well correlated (Figure S4.), indicating PIRA moulin was well-connected to the most hydraulically-efficient regions of the subglacial drainage system that control sliding on sub-diurnal timescales (Andrews et al., 2014). Importantly, before the lake drainage event, ice velocity remained above wintertime background sliding speeds at all times, even when water levels dropped below the piezometer elevation (Figure 2; 19-23 July 2018).

Between 24-30 July 2018, Sentinel-2A and Landsat-8 imagery captured the drainage of ten supraglacial lakes located 8-26 kilometers up-glacier from our instrumented moulin (Fig. 1 Lakes A-J; Figure S1; Table S2). On 25 July at 16:00 local time, moulin water level, ice sliding speeds, and uplift began increasing faster than typical diurnal fluctuations marking the first disturbance to the connected drainage system (Fig. 3ab). An hour after the initial pressure perturbation, glaciohydraulic tremor amplitude sharply increased between 17:15-18:00, suggesting the abrupt arrival of subglacial floodwaters at our site (Fig. 3e). By 18:00, moulin water levels climbed 86 m, reaching 700 m.a.s.l. (approximately 95±7% of overburden). As moulin water levels were quickly rising, along-flow sliding speed peaked to 1.5 m d^{-1} at stations JEME and LMID (Fig. 3b), while the ice was uplifting most rapidly. Maximum event vertical displacement was 10±5 cm and 15±5 cm at JEME and LMID respectively (Fig. 3d). As the subglacial floodwave began to wane and moulin water levels stalled near their highest levels, we observed the onset of exceptionally high amplitude, frequent icequakes at 18:15 (Fig. 3f). Strong icequakes, interpreted to come from the ice sheet bed, continued as the ice sheet regrounded to the bed. By 20:00 moulin water levels and uplift were gradually declining, ice sliding was slowing down, icequake amplitude was getting smaller, and tremor amplitude had halved, all suggesting that most of the floodwaters had drained past our site. Over the next several hours, moulin water levels declined gradually. In contrast, sliding speeds slowed to winter background speeds (hereafter termed simply “background speeds”) by 06:00 on 26 July, even though moulin water levels were still high. Further, similar tremor amplitudes before and after the lake drainage indicate that the subglacial channel’s hydraulic capacity was unchanged (Fig. 3f), agreeing with previous modelling results (Dow et al., 2015). These observations demonstrate that pressure decreases within the most connected parts of the subglacial drainage system do not control ice velocity decreases. For this slowdown to occur, basal traction would need to increase over enough of the bed to counter the high-water pressures in the most connected parts of the drainage system.

For the remainder of the melt season, peak diurnal moulin water levels and sliding speeds remained well-correlated, but, in contrast to the period before the lake drainage, ice velocity minimums recurrently fell to background speeds (Fig. 2; Fig. S4). For example, before the lake drainage (19-25 July), moulin water level fell below the piezometer’s 597 m.a.s.l. elevation while ice velocities remained above background speeds. However, after the lake drainage, ice velocity fell to background speeds while moulin water levels were above the piezometer (600 m.a.s.l. on 5 August and 598 m.a.s.l. on 7 August; Figure S4). This change in the relationship between diurnal minima indicates the increased basal traction triggered by the lake drainage has a lasting effect on ice velocity minima. We recorded a similar progression in 2017, but without seismic observations (Supplementary Materials).

4 Discussion

Given our observations before, during, and after lake drainages in 2017 and 2018, we infer that the slowdown to winter background speeds was caused by increased basal traction following the drainage of water from isolated cavities that became transiently connected during the lake drainage event and not increased channelization.

4.1 Conceptual Model of Flood wave Induced Isolated Cavity Connection

We interpret the results of our study to reflect the following sequence of events. Rapid lake drainage triggered a subglacial floodwave that quickly exceeded the subglacial drainage system’s hydraulic capacity, as evidenced by rapid increases in moulin hydraulic head and ice motion as the floodwave approached our site (Fig. 3). As sliding speed increased, subglacial cavities expanded, forming new connections between linked and previously isolated cavities where cavities grew into each other (Fig. 4a-b). As the distributed drainage system expanded, high-pressure areas expanded across the bed to further increase sliding. Once the subglacial floodwave began to recede, back-pressure dissipated, allowing water injected into the distributed system to drain back towards conduits (Bartholomaus et al., 2007). Water within previously isolated cavities drained through newly formed connections, reducing water pressure within these previously high-pressure cavities (Fig. 4c). Drainage of isolated cavities, therefore, increased basal traction and slowed sliding to background speeds. After the lake drainage event, interconnections formed during the lake drainage event could have persisted, effectively expanding the distributed drainage system. Additionally, some connections may have closed closed-off when water pressures were low (Iken & Truffer, 1997; Murray & Clarke, 1995; Rada & Schoof, 2018), remaining below ice overburden pressure due to the slow timescales of internal meltwater gen-

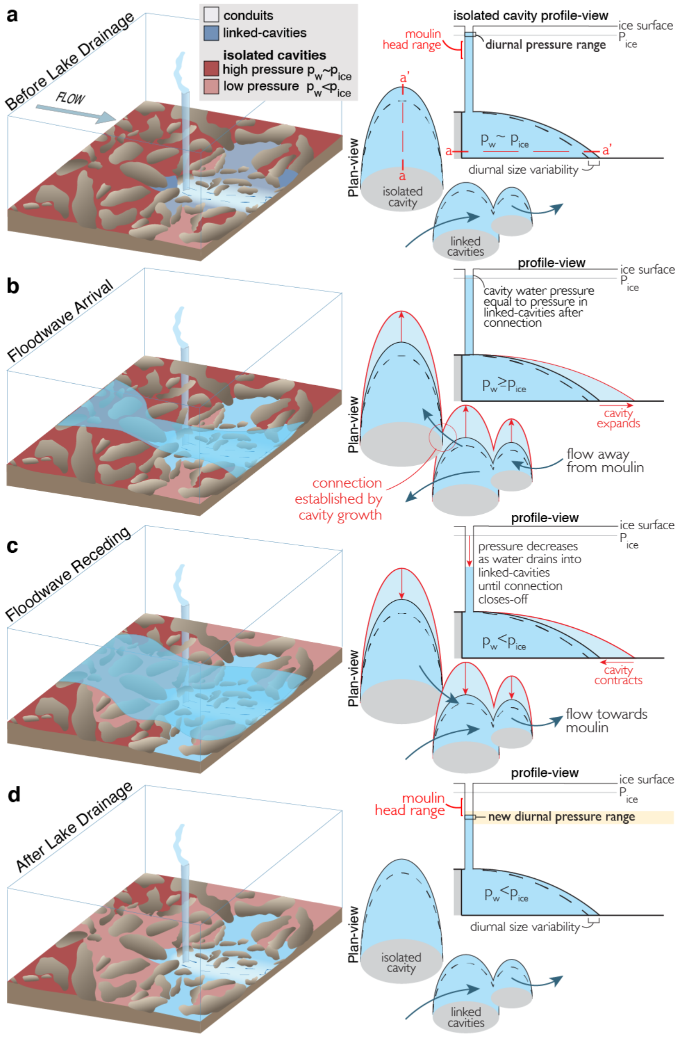

Figure 4. Conceptual model of rapid lake drainages dewatering isolated drainage system. a, Pre-lake drainage: meltwater inputs to moulins drain through subglacial conduits (blue dashed line) which exchange water with nearby linked-cavities (blue). High-pressure isolated cavities occupy a large fraction of the bed with pressure fluctuations opposing those in the connected drainage system. b, Rising limb of floodwave: floodwaters quickly overwhelm conduits, driving water laterally into the distributed system and ice accelerates. Cavities expand and grow into each other at which time water quickly fills and over pressurizes previously isolated cavities. c, Receding-limb of floodwave: water flows through new connections back towards conduits reducing water pressures over a large area of the bed. d, Post-lake drainage: linked-cavities and low-pressure isolated and weakly connected cavities occupy a larger area of the bed, increasing basal traction when compared to pre-lake drainage.

eration required to repressurize the cavity or by maintaining a "weak" connection to the distributed system (Hoffman et al., 2016). As such, a persistent basal traction increase would have been produced as long as most of the drained cavities remained at pressures below ice overburden pressure, resulting in the observed reoccurring slowdown to background sliding speeds.

4.2 Role of Rapid Lake Drainages on GrIS Sliding

While previous studies have emphasized the role of lakes in temporarily increasing sliding speeds, our study suggests rapid lake drainages can trigger rapid isolated cavity drainage following the passage of subglacial floodwaves. Consequently, the role of rapid lake drainages on ice dynamics is ambiguous. On the one hand, lake drainages increase ice velocities by triggering speedups (Selmes et al., 2011; Stevens et al., 2015) and creating stress conditions that form new moulins that deliver meltwater to the bed (Hoffman et al., 2018). On the other hand, our data show lake drainages can decrease ice velocities over large areas by dewatering isolated cavities, explaining the correlation between rapid lake drainages and the onset of seasonal ice deceleration (Andrews et al., 2018).

When compared to other work on isolated cavities on the GrIS (Andrews et al., 2014; Hoffman et al., 2016), our study suggests that seasonal ice dynamics and the onset of ice deceleration may vary depending on whether or not areas of the ice sheet are influenced by rapid lake drainages or only local inputs by moulins. In areas of the ice sheet that are influenced by rapid lake drainages, massive subglacial floodwaves can expand into and connect cavities across large areas of the bed. Dewatering of previously isolated cavities would then drive seasonal ice deceleration (Andrews et al., 2018), potentially early in the melt season. In areas of the ice sheet not influenced by rapidly draining lakes, short-lived increases in melting and meltwater delivery to moulins may create smaller scale, more local flood events that overwhelm the hydraulic capacity of the drainage system connected to a single moulin and drive either the incremental dewatering of isolated cavities or gradual drainage of weakly connected cavities (Andrews et al., 2014; Hoffman et al., 2016).

4.3 Role of Isolated Cavities in Driving GrIS Slowdowns

Neither rapid lake drainages nor the isolated drainage systems are currently considered in the models used to predict the GrIS's sea-level rise contribution. To a large degree, their lack of inclusion stems from the widespread use of alpine glaciers as GrIS analogues. While GrIS ice dynamics have long been interpreted in the context of better-studied alpine glaciers, there are essential differences between the two systems that may limit the applicability of the alpine glacier model to the GrIS. High moulin densities, steep surface slopes, thin ice, and slow creep-closure rates of smaller alpine glaciers allow for dense networks of high-capacity channels. High channel density can lower subglacial water pressure over broad regions of the glacier bed and limit the area available for isolated cavity formation, both of which limit the impacts of isolated cavities on alpine glacier sliding.

On the GrIS, however, low moulin densities likely result in lower subglacial channel density (Banwell et al., 2016), meaning there is more bed area available for isolated cavities to form and influence ice dynamics. Shallow surface slopes, thick ice, and fast creep-closure rates, characteristic of much of the GrIS ablation zone, may limit the drainage system's ability to increase its hydraulic capacity quickly enough to drain enough water from the distributed system and lower water pressure over large areas of the bed. Accordingly, GrIS dynamics may be more sensitive to sustained meltwater inputs than previously thought.

5 Conclusion

Direct measurements of water pressure along a subglacial flow-path showed that large influxes of meltwater from lake drainages can drain isolated cavities and slow sliding speeds without increasing the drainage system's efficiency. Building upon previous studies (Andrews et al., 2014; Hoffman et al., 2016), these results demonstrate that decreasing ice velocity has been mainly incorrectly attributed to the subglacial drainage system's ability to adjust its hydraulic capacity in response to meltwater inputs readily. As a result, ice dynamics of the GrIS may be especially vulnerable to sustained meltwater inputs, even where efficient subglacial drainage does exist. Future modelling efforts must incorporate the response of unchannelized parts of the subglacial drainage system to meltwater inputs in order to achieve accurate predictions of future GrIS contributions to sea-level rise.

Acknowledgments

This work was supported by the United States National Science Foundation grant number 1604022. The GNSS base station and on-ice stations were provided by UNAVCO in collaboration with N.S.F. Logistical support was provided by CH2MHill Polar Services. The authors declare there are no conflicts of interest with regard to finances or with the results of this paper. We thank Victoria Siegel, Charles Breithaupt, and others for their assistance in the field.

Data Availability Statement

The data associated with this manuscript can be accessed through the ArcticData.io platform [doi:10.18739/A2M03XZ13, doi:10.18739/A2CF9J745.], (Mejia, Trunz, Covington, Gulley, & Breithaupt, 2020; Mejia, Trunz, Covington, & Gulley, 2020).

References

Andrews, L. C., Catania, G. A., Hoffman, M. J., Gulley, J. D., Lüthi, M. P., Ryser, C., ... Neumann, T. A. (2014). Direct observations of evolving subglacial drainage beneath the Greenland Ice Sheet. *Nature*, *514*(7520), 80–83. Retrieved from `http://www.nature.com/doifinder/10.1038/nature13796` doi: 10.1038/nature13796

Andrews, L. C., Hoffman, M. J., Neumann, T. A., & Catania, G. A. (2018). Seasonal Evolution of the Subglacial Hydrologic System Modified by Supraglacial Lake Drainage in Western Greenland. *Journal of Geophysical Research : Earth Surface*, *123*, 1479–1496. doi: 10.1029/2017JF004585

Banwell, A. F., Hewitt, I. J., Willis, I. C., & Arnold, N. S. (2016). Moulin density controls drainage development beneath the Greenland ice sheet. *Journal of Geophysical Research: Earth Surface*, *121*(12), 2248–2269. doi: 10.1002/2015JF003801

Bartholomaus, T. C., Anderson, R. S., & Anderson, S. P. (2007). Response of glacier basal motion to transient water storage. *Nature Geoscience*, *1*, 33–37. doi: 10.1038/ngeo.2007.52

Bartholomaus, T. C., Larsen, C. F., Amundson, J. M., O'Neel, S., Walter, J. I., & West, M. E. (2015). Subglacial discharge at tidewater glaciers revealed by seismic tremor. *Geophysical Research Letters*, *42*, 6391–6398. doi: 10.1002/2015GL064590.Received

Bartholomew, I., Nienow, P. W., Sole, A. J., Mair, D., Cowton, T., & King, M. A. (2012). Short-term variability in Greenland Ice Sheet motion forced by time-varying meltwater drainage: Implications for the relationship between subglacial drainage system behavior and ice velocity. *Journal of Geophysical Research: Earth Surface*, *117*(3), 1–17. doi: 10.1029/2011JF002220,2012

Chandler, D. M., Wadham, J., Lis, G., Cowton, T., Sole, A. J., Bartholomew, I.,

... Hubbard, A. (2013). Evolution of the subglacial drainage system beneath the Greenland Ice Sheet revealed by tracers. *Nature Geoscience*, *6*(3), 195–198. Retrieved from http://dx.doi.org/10.1038/ngeo1737 doi: 10.1038/ngeo1737

Colgan, W. T., Rajaram, H., Anderson, R. S., Steffen, C., Zwally, H. J., Phillips, T., & Abdalati, W. (2011). The annual glaciohydrology cycle in the ablation zone of the Greenland ice sheet: Part 1. Hydrology model. *Journal of Glaciology*, *57*(204), 51–64. doi: 10.3189/2012JoG11J081

Dow, C. F., Kulessa, B., Rutt, I., Tsai, V. C., Pimentel, S., Doyle, S. H., ... Hubbard, A. (2015). Modeling of subglacial hydrological development following rapid supraglacial lake drainage. *Journal of Geophysical Research : Earth Surface*, *120*, 1127–1147. doi: 10.1002/2014JF003333.Received

Gulley, J. D., Grabiec, M., Martin, J. B., Jania, J., Catania, G. A., & Glowacki, P. S. (2012). The effect of discrete recharge by moulins and heterogeneity in flow-path efficiency at glacier beds on subglacial hydrology. *Journal of Glaciology*, *58*(211), 926–940. doi: 10.3189/2012JoG11J189

Herring, T., King, R. W., & McClusky, S. C. (2010). Introduction to GAMIT/GLOBK. *Mass. Inst. of Technol., Cambridge, Mass.*

Hoffman, M. J., Andrews, L. C., Price, S. F., Catania, G. A., Neumann, T. A., Lüthi, M. P., ... Morriss, B. (2016). Greenland subglacial drainage evolution regulated by weakly connected regions of the bed. *Nature Communications*, *7*, 13903. Retrieved from http://www.nature.com/doifinder/10.1038/ncomms13903 doi: 10.1038/ncomms13903

Hoffman, M. J., Catania, G. A., Neumann, T. A., Andrews, L. C., & Rumrill, J. A. (2011). Links between acceleration, melting, and supraglacial lake drainage of the western Greenland Ice Sheet. *Journal of Geophysical Research: Earth Surface*, *116*(4), 1–16. doi: 10.1029/2010JF001934

Hoffman, M. J., Perego, M., Andrews, L. C., Catania, G. A., Price, S. F., Lüthi, M. P., ... Johnson, J. V. (2018). Widespread Moulin Formation During Supraglacial Lake Drainages in Greenland. *Geophysical Research Letters*, *45*, 778–788. doi: 10.1002/2017GL075659

Howat, I. M., Tulaczyk, S. M., Waddlngton, E. D., & Björnsson, H. (2008). Dynamic controls on glacier basal motion inferred from surface ice motion. *Journal of Geophysical Research*, *113*(F3), F03015. Retrieved from http://doi.wiley.com/10.1029/2007JF000925 doi: 10.1029/2007JF000925

Iken, A., & Truffer, M. (1997). The relationship between subglacial water pressure and velocity of Findelengletscher, Switzerland, during its advance and retreat. *Journal of Glaciology*, *43*(144), 328–338. doi: 10.1017/CBO9781107415324.004

Lliboutry, L. A. (1968). Local friction laws for glaciers: A critical review and new openings. *Journal of Glaciology*, *23*(89), 67–95.

Meierbachtol, T. W., Harper, J. T., Humphrey, N. F., & Wright, P. J. (2016). Mechanical forcing of water pressure in a hydraulically isolated reach beneath Western Greenland's ablation zone. *Annals of Glaciology*, *57*(72), 62–70. doi: 10.1017/aog.2016.5

Mejia, J., Trunz, C., Covington, M. D., & Gulley, J. D. (2020). *Meteorological data from two on-ice weather stations at 780 and 950 m asl elevations in the ablation area of Sermeq Avannarleq, West Greenland from 2017-2018.* Arctic Data Center. Retrieved from https://arcticdata.io/catalog/view/doi%3A10.18739%2FA2CF9J745 doi: 10.18739/A2CF9J745.

Mejia, J., Trunz, C., Covington, M. D., Gulley, J. D., & Breithaupt, C. (2020). *Moulin hydrological measurements from Sermeq Avannarleq, West Greenland Ice Sheet from 2017-2018.* Arctic Data Center. Retrieved from https://arcticdata.io/catalog/view/doi:10.18739/A2M03XZ13 doi: 10.18739/A2M03XZ13.

Morlighem, M., Williams, C. N., Rignot, E., An, L., Arndt, J. E., Bamber, J. L., ... Zinglersen, K. B. (2017). BedMachine v3: Complete Bed Topography and Ocean Bathymetry Mapping of Greenland From Multibeam Echo Sounding Combined With Mass Conservation. *Geophysical Research Letters*, *44*(21), 051–11. doi: 10.1002/2017GL074954

Morriss, B. F., Hawley, R. L., Chipman, J. W., Andrews, L. C., Catania, G. A., Hoffman, M. J., ... Neumann, T. A. (2013). A ten-year record of supraglacial lake evolution and rapid drainage in West Greenland using an automated processing algorithm for multispectral imagery. *Cryosphere*, *7*(6), 1869–1877. doi: 10.5194/tc-7-1869-2013

Murray, T., & Clarke, G. K. C. (1995). Black-box modeling of the subglacial water system. *Journal of Geophysical Research: Solid Earth*, *100*(B6), 10231–10245. doi: 10.1029/95jb00671

Rada, C., & Schoof, C. (2018). Channelized, distributed, and disconnected: Subglacial drainage under a valley glacier in the Yukon Subglacial drainage controls on basal sliding View project Channelized, distributed, and disconnected: subglacial drainage under a valley glacier in the Yu. *The Cryosphere*, *12*, 2609–2636. Retrieved from `https://doi.org/10.5194/tc-12-2609-2018` doi: 10.5194/tc-12-2609-2018

Roeoesli, C., Helmstetter, A., Walter, F., & Kissling, E. (2016). Meltwater influences on deep stick-slip icequakes near the base of the Greenland Ice Sheet. *Journal of Geophysical Research : Earth Surface*, *121*, 223–240. doi: 10.1002/2015JF003601.Received

Ryser, C., Lüthi, M. P., Andrews, L. C., Catania, G. A., Funk, M., & Hawley, R. L. (2014). Caterpillar-like ice motion in the ablation zone of the Greenland ice sheet. *Journal of Geophysical Research : Earth Surface*, *119*, 2258–2271. doi: 10.1002/2013JF003067.Received

Schwanghart, W., & Kuhn, N. J. (2010). TopoToolbox: A set of Matlab functions for topographic analysis. *Environmental Modelling and Software*. doi: 10.1016/j.envsoft.2009.12.002

Selmes, N., Murray, T., & James, T. D. (2011). Fast draining lakes on the Greenland Ice Sheet. *Geophysical Research Letters*, *38*(15), 1–5. doi: 10.1029/2011GL047872

Sole, A. J., Nienow, P. W., Bartholomew, I., Mair, D., Cowton, T., Tedstone, A. J., & King, M. A. (2013). Winter motion mediates dynamic response of the Greenland Ice Sheet to warmer summers. *Geophysical Research Letters*, *40*(15), 3940–3944. doi: 10.1002/grl.50764

Steffen, C., Box, J. E., & Abdalati, W. (1996). Greenland Climate Network: GC-Net. *Cold Regions Research and Engineering Laboratory*, *CRREL Spec*, 98–103.

Stevens, L. A., Behn, M. D., McGuire, J. J., Das, S. B., Joughin, I., Herring, T., ... King, M. a. (2015). Greenland supraglacial lake drainages triggered by hydrologically induced basal slip. *Nature*, *522*(7554), 73–76. Retrieved from `http://www.nature.com/doifinder/10.1038/nature14480` doi: 10.1038/nature14480

Stone, D., & Clarke, G. K. C. (1996). in Situ Measurements of Basal Water Quality and Pressure As an Indicator of the Character of Subglacial Drainage Systems. *Hydrological Processes*, *10*(4), 615–628. doi: 10.1002/(sici)1099-1085(199604)10:4⟨615::aid-hyp395⟩3.3.co;2-d

Sundal, A. V., Shepherd, A., Nienow, P. W., Hanna, E., Palmer, S., & Huybrechts, P. (2011). Melt-induced speed-up of Greenland ice sheet offset by efficient subglacial drainage. *Nature*, *469*(7331), 521–524. Retrieved from `http://dx.doi.org/10.1038/nature09740` doi: 10.1038/nature09740

Virtanen, P., Gommers, R., Oliphant, T. E., Haberland, M., Reddy, T., Cournapeau, D., ... Vázquez-Baeza, Y. (2020). SciPy 1.0: fundamental algorithms for scientific computing in Python. *Nature Methods*, *17*, 261–272. doi: 10.1038/s41592-019-0686-2

Walder, J. S. (1986). Hydraulics of subglacial cavities. *Journal of Glaciology*, *32*(112), 439–445. Retrieved from `http://www.igsoc.org:8080/journal/32/112/igs_journal_vol32_issue112_pg439-445.pdf`

Williamson, A. G., Arnold, N. S., Banwell, A. F., & Willis, I. C. (2017). A Fully Automated Supraglacial lake area and volume Tracking ("FAST") algorithm: Development and application using MODIS imagery of West Greenland. *Remote Sensing of Environment*, *196*, 113–133. Retrieved from `https://doi.org/10.1016/j.rse.2017.04.032` doi: 10.1016/j.rse.2017.04.032

Xie, S., Law, J., Russell, R., Dixon, T. H., Lembke, C., Malservisi, R., . . . Chen, J. (2019). Seafloor Geodesy in Shallow Water With GPS on an Anchored Spar Buoy. *Journal of Geophysical Research: Solid Earth*, *124*(11), 12116–12140. doi: 10.1029/2019JB018242

Supporting Information for "Isolated cavities dominate Greenland Ice Sheet ice dynamic response to lake drainages."

J. Z. Mejia[1], J. D. Gulley[1], C. Trunz[2], M. D. Covington[2], T. C. Bartholomaus[3], S. Xie[4], T. Dixon[1]

[1]Department of Geosciences, University of South Florida, 4202 E. Fowler Ave. Tampa, FL 33620.

[2]Department of Geosciences, University of Arkansas, 1 University of Arkansas, Fayetteville, AR 72701

[3]Department of Geological Sciences, University of Idaho, 875 Perimeter Drive, Moscow, ID 83844

[4]Scripps Institution of Oceanography, University of California San Diego, 9500 Gilman Drive, MC 0225, La Jolla, CA 92093

Contents of this file

1. Text S1 to S5
2. Figures S1 to S7
3. Tables S1 to S2

Introduction

Corresponding author: J. Z. Mejia, Department of Geosciences, University of South Florida, 4202 E. Fowler Dr., Tampa, FL 33620, USA. (jessicamejia@usf.edu)

This supplement provides additional information relating to the main text and details on methodology. **Text S1** elaborates on moulin instrumentation. **Text S2** describes methods used in processing GNSS station data, calculating ice velocities, and determining uplift. **Text S3** elaborates on the procedure used to determine tremor amplitudes and ice quakes from our seismic station SELC. **Text S4** describes the methodology used to determine subglacial routing where **Figure S2** shows the bed topography used in this calculation. **Text S5** and **Figures S6** and **S7** describe our observations during the 2017 lake drainage event at the same location.

Figure S1 shows the satellite imagery constraints on the 2018 lake drainage events. **Figure S3** shows the extended timeseries data over the 2018 melt season, with the addition of surface air temperatures and **Figure S4** shows the relationship between moulin hydraulic head and ice velocity. **Figure S5.** shows the local atmospheric pressure correction. Additionally, **Table S1.** shows locations of our instrumentation and field site while **Table S2.** provides specific information regarding each supraglacial lake drainage.

Text S1.

Moulin instrumentation:

To convert the sensor measurements of water pressure (P_w) to hydraulic head (h) we subtract the piezometer's depth from the GNSS reported ice surface elevation to determine the sensor elevation (z_{sensor}) in meters above sea level. Then, we calculate hydraulic head using the following which assumes a vertical moulin shaft, consistent with uppermost ~ 30 m:

$$h = \frac{P_w}{\rho_w g} + z_{sensor} \tag{1}$$

where ρ_w is the density of water and g is acceleration due to gravity. We estimate an error of 20 m in our absolute moulin head measurements, arising from the uncertainty in the sensor elevation as described in detail in Andrews et al. (2014). Importantly, error in absolute moulin head does not apply to our measurements of relative change (e.g. diurnal variations). We represent moulin hydraulic head as measured from sea-level to allow for comparison with existing datasets and to avoid using poorly constrained bed elevations ($\sim$ 100-meter uncertainty).

We use atmospheric pressures recorded by the GC-NET weather station JAR1 (Steffen et al., 1996), located approximately 5 kilometers northeast of our instrumented moulins JEME (2017) and PIRA (2018). Due to instrument failure, atmospheric pressure variations were not available during the 2018 melt season to correct PIRA hydraulic head. However, the additional error introduced to our 2018 water pressure record is likely small as evidenced by the 2017 correction (Figure S5.) where atmospheric pressure variability is on the order of centimeters (std=0.05 m) while moulin hydraulic head varies on the order of tens of meters (std=34.5 m).

Text S2.

Ice velocity and uplift determination:

Post-processed positions were then imported to Python for further analysis (Virtanen et al., 2020). We transformed into the along-flow and across-flow directions for each station. Before calculating velocities, we filtered positions to reduce spurious signals resulting from GNSS uncertainties by applying a 6-hour rolling mean to each position time series. Velocity is calculated along each component of motion by differencing 2-

hour separated positions. We determined winter background speeds by averaging velocity calculated during periods of continuous measurements between March and May 2018, before the onset of the melt. Formal error is estimated during processing are 1-2 cm in the horizontal direction and 4-5 cm vertically, with a velocity uncertainty of 0.024 m d^{-1}.

Measured vertical ice motion is attributed to a combination of flow along a sloping bed, strain thickening or thinning, and bed separation caused by cavity opening or till dilation where subglacial sediments are present (Howat et al., 2008). To account for changes in elevation associated with bed slope, we detrend the vertical component of motion with respect to distance traveled in the long-flow direction using the linear fit before the melt season when strain and cavity opening should be constant. We transform detrended vertical motion back to the time domain to produce the uplift time series. Consequently, this uplift time series accounts for bed separation due to cavity opening, strain thickening or thinning, and sediment dilation. Previous studies close to our field site (Andrews et al., 2014; Hoffman et al., 2011) have documented significant bed separation over short timescales, suggesting increased bed separation due to cavity growth is likely a significant source of the (> 10 cm) uplift observed during each lake drainage event.

Text S3.

Seismic Analysis:

Glaciohydraulic tremor is characterized by long-duration, low amplitude background seismic noise that varies slowly without clear onset or termination. The amplitude of these ground variations depends on both the flux and the pressure gradient of turbulently-flowing water within efficient, well-connected conduits. We characterized the glaciohydraulic tremor amplitude using two different metrics: 1) the median power between 1.5-10 Hz calculated within 1-hr data windows (Bartholomaus et al., 2015), and 2) as the 20th percentile amplitude of enveloped, 10-minute, seismic waveforms, high-pass filtered above 2 Hz. This 20th percentile amplitude was chosen to be well below the higher percentile values that may represent distinct ice fracturing events-equivalent results are obtained for other percentile metrics below approximately 50. Because both measures of glaciohydraulic tremor produced qualitatively similar time series, but the second approach was tailored to work with better temporal resolution, we present the 20th percentile envelope analysis approach.

Distinct from the slowly varying timeseries of glaciohydraulic tremor are distinct, impulsive “icequakes” that typically are found at frequencies greater than 10 Hz. These icequakes are produced by ice fracture events (e.g., crevassing) at the glacier surface, englacially, or at the glacier bed. We quantify the strength of these locally recorded seismic events by the maximum seismic amplitude recorded at our station within 10-minute moving windows. The maximum seismic amplitude depends both on the scale of an event (slip length, stress reduction during the event, and surface area of the fracture surface) and the distance between the event origin and the sensor. Additionally, we examined the seven largest seismic events that occur during the 25 July 2018. These events each consist of paired seismic arrivals on each of three station channels that are consistent with P- and S-waves, very high frequency content ($> 50 - 100$ Hz), inter-phase arrival times that are consistent with a source 500-1000 m from the station (such as the bed), and mostly with downward first P-wave motions, consistent with some kind of crack closing. Some of these high frequency events had a low-frequency coda consistent with the presence of water. So, while we lack the ability to definitively locate these events, we believe that the high-amplitude icequakes late on 25 July are best explained as ice fracture events at the ice sheet bed.

Text S4.

Subglacial routing via hydraulic potential gradients.:

Subglacial routing via hydraulic potential gradients. We estimate subglacial hydraulic potential gradients (ϕ) following:

$$\phi = \rho_w g z_b + P_w \tag{2}$$

where ϕ_w is the density of water, g is acceleration due to gravity, z_b is bed elevation, and P_w is subglacial water pressure, assumed to be equal to ice overburden pressure (or $\rho g h$, where ρ_i is ice density and h is the ice thickness). Surface and bed elevations (Figure S2) are derived from the BedMachine Greenland v3 dataset (Morlighem et al., 2017) with a 150 m-resolution (true resolution 400 m). This calculation requires the assumption that subglacial water pressures are at overburden throughout the domain during conduit formation. Once conduit flow paths are established, they can expand by melting and contract by creep closure but their locations are unlikely to change (Gulley et al., 2012). We determine flow paths by calculating flow accumulation along subglacial hydropotential gradients using the MATLAB topotools toolbox (Schwanghart & Kuhn, 2010). We use surface and bed elevations at points spaced 50-m along the hydropotential flow path connecting Lake E to the terminus (bold pink line) for the bed profile in Figure 1c.

While our observations show a direct connection between a draining supraglacial lake and a moulin located over eight kilometers downglacier, instrument records suggest the floodwave modified an even larger area of the subglacial drainage system. The similarity between the GNSS station response to each lake drainage event indicates the lateral extent of the floodwave was at least 500 m, which is approximately equivalent to the ice thickness in this area. We argue that our observations reflect the lower limit on the area of the isolated drainage system dewatered by the subglacial floodwave. It is likely that similar alterations to the subglacial drainage system occurred at downglacier locations as the floodwave continued propagating towards the coast.

Text S5.

Isolated cavities dominate Greenland Ice sheet dynamic response to lake drainage:

On 21 July 2017, we instrumented JEME moulin with a pressure transducer that was anchored 350 m below the ice surface. By July 2018, moulin JEME had been advected 90 m downglacier, consistent with measured annual ice displacement of approximately 90 m a^{-1}. On 10 July 2018, we instrumented the new moulin, PIRA, which opened in the same position on the ice sheet as JEME the year before. In 2017, Sentinel-2A and Landsat 8 imagery captured three supraglacial lake drainages between 26-27 July (**Figure S6**; Lakes A and B; **Figure S7**). On 27 July at 02:30UTC, moulin water levels deviated from their nightly decline as the subglacial floodwave created by the lake drainages approached our site. By 04:30 UTC, moulin water level had jumped more than 60 m (about 13

Over the week following the lake drainage event minimum moulin water levels declined. By 3 August, the diurnal minimum moulin water level was 60 m lower than after the lake drainage event when ice velocities initially fell to wintertime background speeds. Despite this significant reduction in minimum moulin water level (for comparison, during the lake drainage event moulin water levels increased by 60 m) minimum ice velocity remained at winter background speeds, unaffected by the falling pressures within the active drainage system. This observation contradicts the behavior expected if increased efficiency of the channelized drainage system slowed sliding speeds. Therefore, while increased pressurization of the active drainage system reduced basal traction to drive diurnal acceleration, declining pressures in the active drainage did not reduce minimum sliding speeds. Instead, these observations indicate the state of the isolated drainage system governed the lower limit of sliding speeds.

References

Andrews, L. C., Catania, G. A., Hoffman, M. J., Gulley, J. D., Lüthi, M. P., Ryser, C., … Neumann, T. A. (2014). Direct observations of evolving subglacial drainage beneath the Greenland Ice Sheet. *Nature*, *514* (7520), 80–83. Retrieved from `http://www.nature.com/doifinder/10.1038/nature13796` doi: 10.1038/nature13796

Bartholomaus, T. C., Larsen, C. F., Amundson, J. M., O'Neel, S., Walter, J. I., & West, M. E. (2015). Subglacial discharge at tidewater glaciers revealed by seismic tremor. *Geophysical Research Letters*, *42*, 6391–6398. doi: 10.1002/2015GL064590.Received

Gulley, J. D., Grabiec, M., Martin, J. B., Jania, J., Catania, G. A., & Glowacki, P. S. (2012). The effect of discrete recharge by moulins and heterogeneity in flow-path efficiency at glacier beds on subglacial hydrology. *Journal of Glaciology*, *58*(211), 926–940. doi: 10.3189/2012JoG11J189

Hoffman, M. J., Catania, G. A., Neumann, T. A., Andrews, L. C., & Rumrill, J. A. (2011). Links between acceleration, melting, and supraglacial lake drainage of the western Greenland Ice Sheet. *Journal of Geophysical Research: Earth Surface*, *116*(4), 1–16. doi: 10.1029/2010JF001934

Howat, I. M., Tulaczyk, S. M., Waddlngton, E. D., & Björnsson, H. (2008). Dynamic controls on glacier basal motion inferred from surface ice motion. *Journal of Geophysical Research*, *113*(F3), F03015. Retrieved from `http://doi.wiley.com/10.1029/2007JF000925` doi: 10.1029/2007JF000925

Morlighem, M., Williams, C. N., Rignot, E., An, L., Arndt, J. E., Bamber, J. L., … Zinglersen, K. B. (2017). BedMachine v3: Complete Bed Topography and Ocean Bathymetry Mapping of Greenland From Multibeam Echo Sounding Combined With Mass Conservation. *Geophysical Research Letters*, *44*(21), 051–11. doi: 10.1002/2017GL074954

Morriss, B. F., Hawley, R. L., Chipman, J. W., Andrews, L. C., Catania, G. A., Hoffman, M. J., … Neumann, T. A. (2013). A ten-year record of supraglacial lake evolution and rapid drainage in West Greenland using an automated processing algorithm for multispectral imagery. *Cryosphere*, *7*(6), 1869–1877. doi: 10.5194/tc-7-1869-2013

Schwanghart, W., & Kuhn, N. J. (2010). TopoToolbox: A set of Matlab functions for topographic analysis. *Environmental Modelling and Software*. doi: 10.1016/j.envsoft.2009.12.002

Steffen, C., Box, J. E., & Abdalati, W. (1996). Greenland Climate Network: GC-Net. *Cold Regions Research and Engineering Laboratory*, *CRREL Spec*, 98–103.

Virtanen, P., Gommers, R., Oliphant, T. E., Haberland, M., Reddy, T., Cournapeau, D., ... Vázquez-Baeza, Y. (2020). SciPy 1.0: fundamental algorithms for scientific computing in Python. *Nature Methods*, *17*, 261–272. doi: 10.1038/s41592-019-0686-2

Williamson, A. G., Arnold, N. S., Banwell, A. F., & Willis, I. C. (2017). A Fully Automated Supraglacial lake area and volume Tracking ("FAST") algorithm: Development and application using MODIS imagery of West Greenland. *Remote Sensing of Environment*, *196*, 113–133. Retrieved from `https://doi.org/10.1016/j.rse.2017.04.032` doi: 10.1016/j.rse.2017.04.032

Table S1. Field instrumentation locations

	Latitude °N	Longitude °E	Elevation (m)	Ice thickness (m)	
JEME & PIRA moulins	69.4741	-49.8232	779	503	supraglacial stream entering from east
JEME GNSS 2018	69.4738	-49.8249	797	503	~ 90 m southwest (downglacier) from PIRA moulin
LMID GNSS	69.4708	-49.8189	796	514	uncrevassed, local high
JNIH GNSS	69.4684	-49.8318	790	547	uncrevassed, near small supraglacial stream and moulin
LC weather station	69.4727	-49.8263	777	512	uncrevassed, supraglacial streams to north and south
LC seismic station	69.4734	-49.8208	781	498	only active during 2018.

Lake	Max Area (km^2)	Volume** (m^3)	Latitude °N	Longitude °E	Elevation (m.a.s.l.)	Ice thickness (m)	Distance (km) Direct	Distance (km) Subglacial
A 63*	(0.633) 0.946	(4.9)8.6×10^5	69.4537	-49.6247	888	728	7.4	8.9
B 59	(0.331) 0.362	(2.4)2.6×10^5	69.4710	-49.6272	930	673	7.4	9.8
C 68	1.963	2.8×10^6	69.4355	-49.5297	913	882	12.3	13.4
D 57	0.490	3.6×10^5	69.4764	-49.3836	1021	918	17.4	22.2
E 50	1.365	1.5×10^6	69.4897	-49.2151	1100	1065	23.8	33.3
F 43	1.350	1.5×10^6	69.5343	-49.1291	1131	1120	27.9	40.2
G 45	0.493	3.6×10^5	69.5253	-49.1952	1159	1020	25.2	37.6
H 38	0.701	5.6×10^5	69.5496	-49.1801	1159	1100	26.5	40.6
I 35	2.300	3.8×10^6	69.5724	-49.2104	1146	1020	21.5	33.7
J 33	1.224	1.3×10^6	69.5680	-49.3410	1115	1160	26.4	37.6

* numbers correspond with Morriss et al. (2013) naming conventions

** values have an associated error of 0.420×10^6 m^3.

() denote values associated with 2017 lake drainage events.

Table S2. Volume estimated using an area-to-volume scaling relationship for the Paakitsoq region (Williamson et al., 2017).

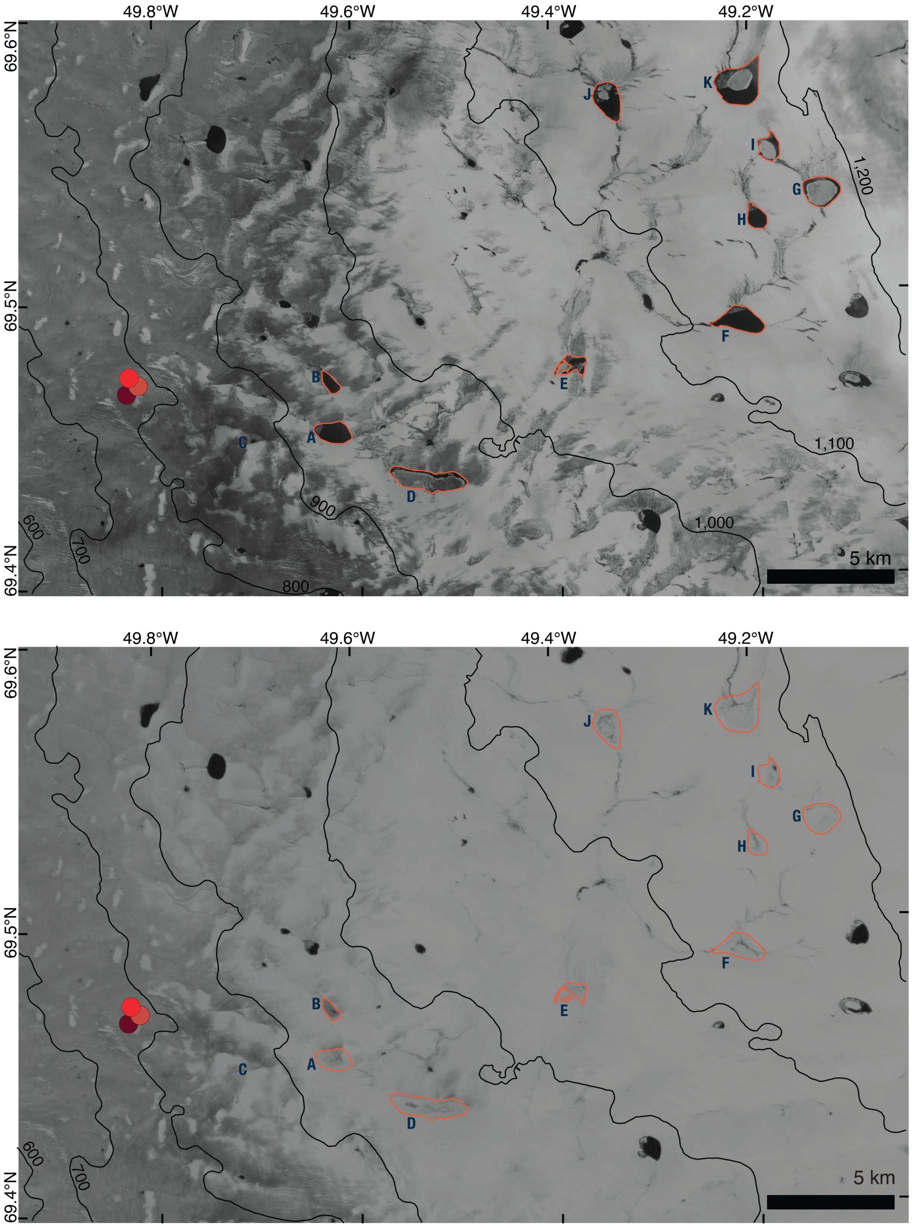

Figure S1. Satellite imagery constrains on 2018 lake drainage. (a) Copernicus Sentinel image acquired on 24 July 2018 at 15:29:11 UTC showing the maximum extents of supraglacial lakes A-J (red outlines), with the location of our instruments (red circles). (b) Landsat-8 image acquired on 30 July 2018 at 14:59:53 UTC showing the drainage of lakes A-J, maximum extents same as in a. Surface elevation contours (m) are from BedMachine-v3. Data available from the U.S. Geological Survey

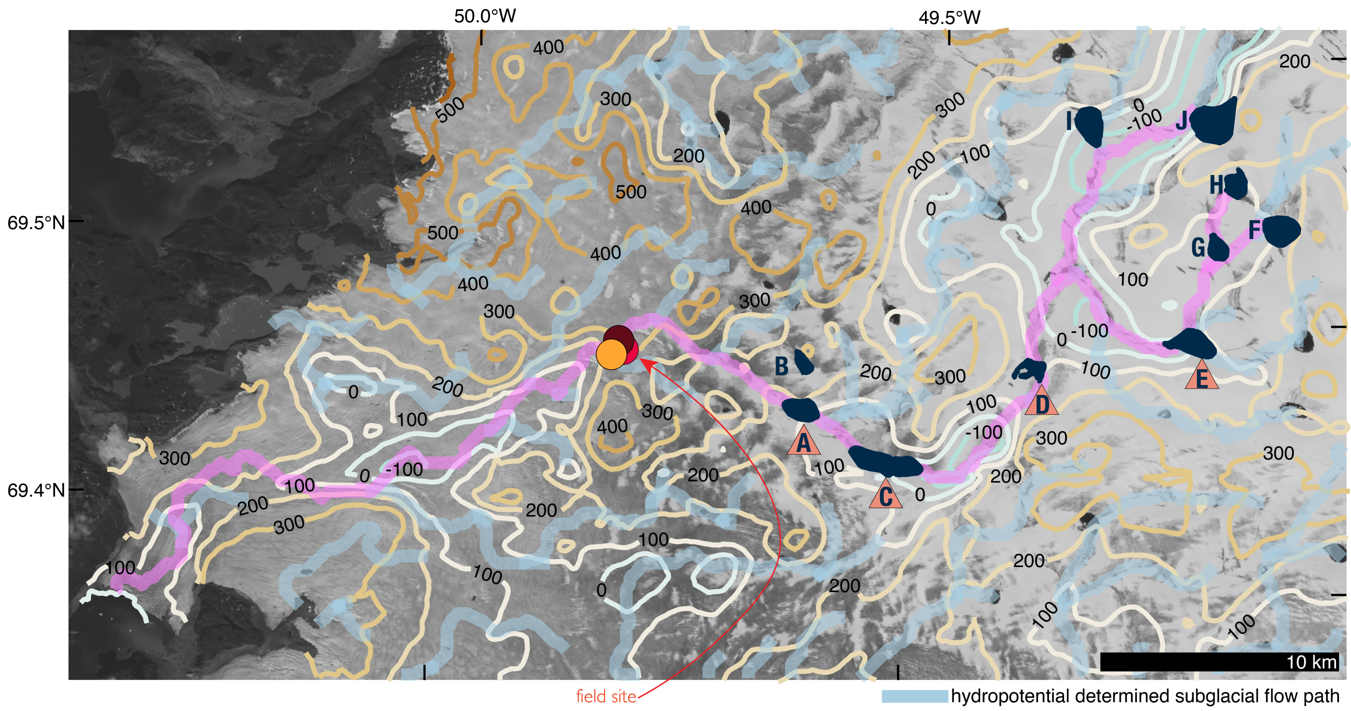

Figure S2. Bed topography and hydropotential predicted subglacial flow routing. BedMachine derived bed elevation contours are shown in meters. Subglacial flow routing from hydropotential gradients is shown in light blue. Supraglacial lakes mentioned in the main text are labeled and their maximum extents are marked in navy.

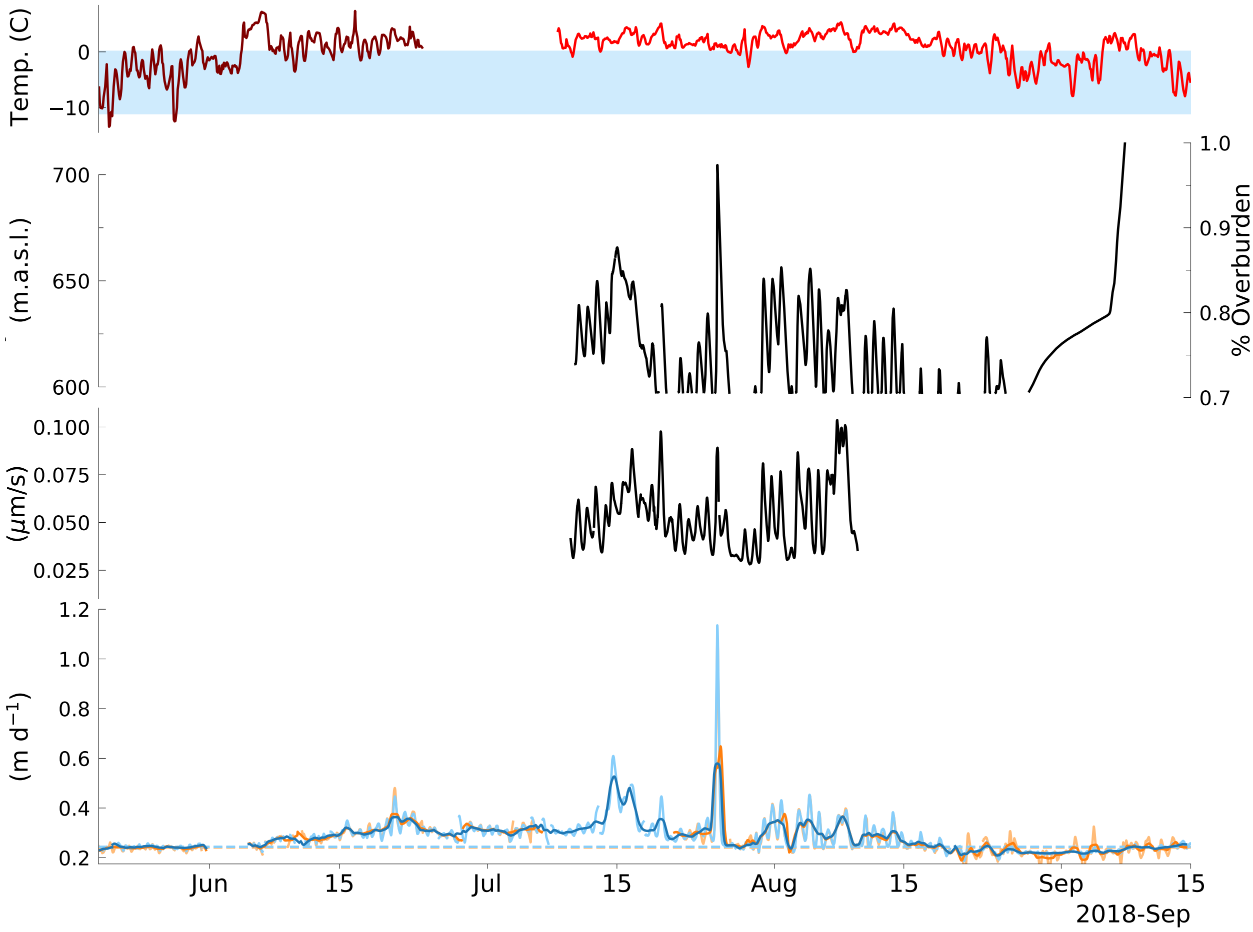

Figure S3. (a) Surface air temperature recorded at LOWC weather station (red) and the GC-NET station JAR1 (maroon). (b) Moulin hydraulic head in m.a.s.l. and fraction of overburden for an ice thickness of 503 m. (c) Glaciohydraulic tremor amplitude smoothed with a 6-h rolling mean. (d) Along-flow ice velocity measured at stations JEME (orange) and LMID (blue). Light colors are smoothed with a 6-h rolling mean to show diurnal variability and light colors are smoothed with a 24-hr rolling mean emphasize the slowdown following the mid-season lake drainage event. Blue and orange dashed lines mark winter background sliding speeds.

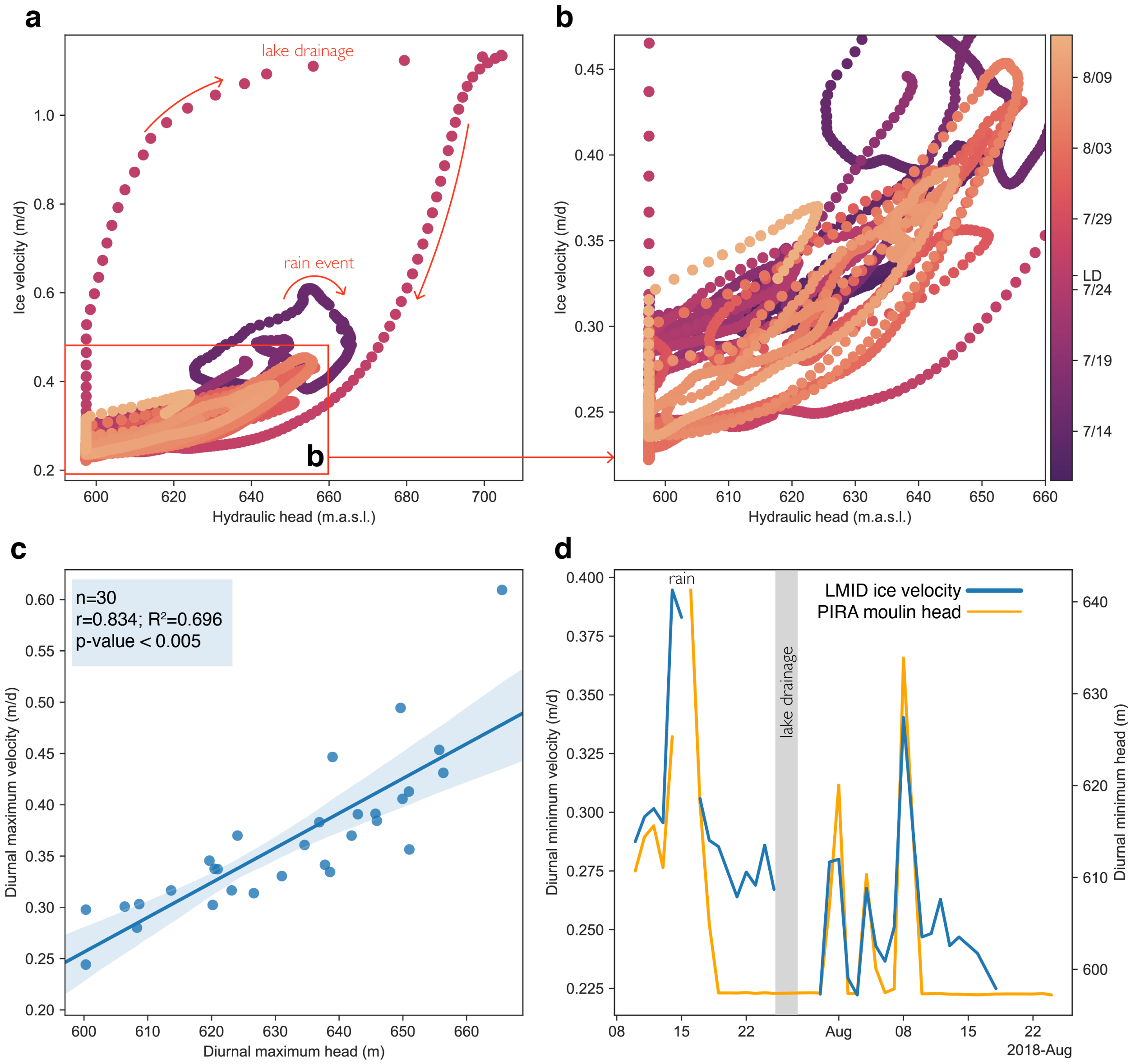

Figure S4. (a-b) Moulin hydraulic head and ice velocity variations coloring reflects the date of the measurements. A zoom in to diurnal variations is shown in b. Diurnal variations move in a clock-wise pattern. (c) Linear regression between diurnal maximum moulin hydraulic head and ice velocity ($n = 30, r = 0.834, p < 0.05$). (d) Diurnal minimum ice velocity and moulin head plotted though time.

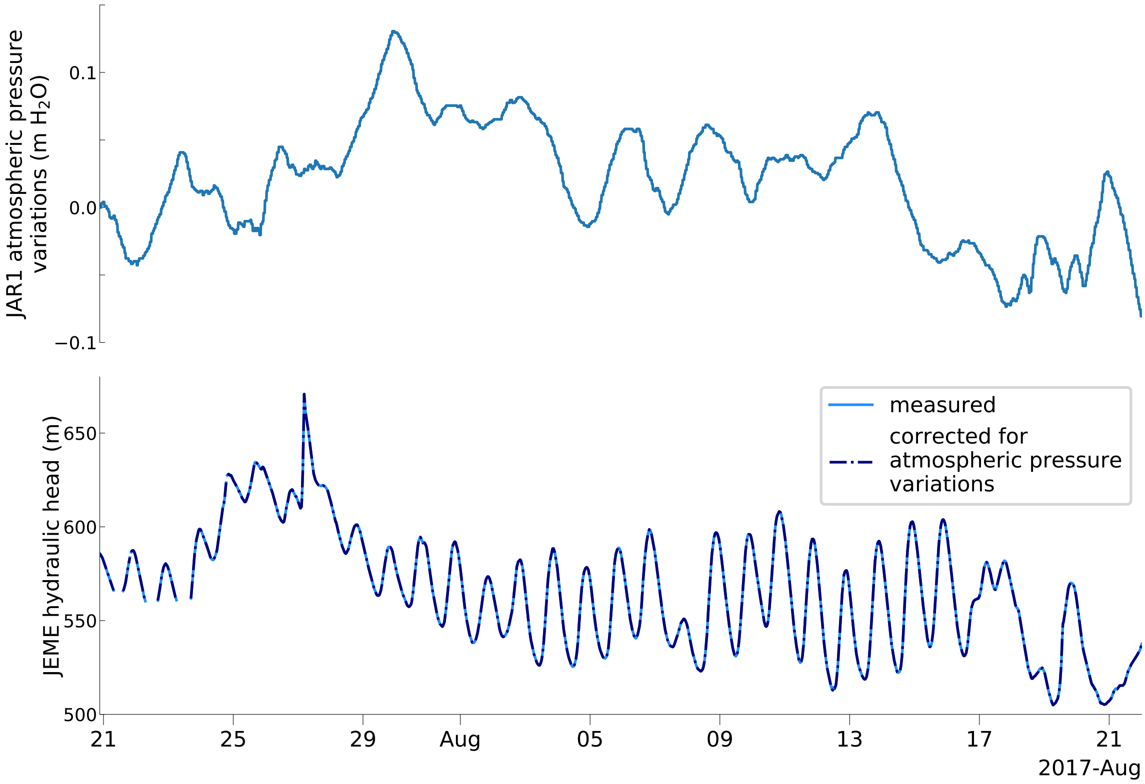

Figure S5. 2017 Atmospheric pressure variability. (a) Atmospheric pressure measured at JAR1 less the atmospheric pressure at the time JEME moulin was instrumented (9.2422 m H2O). (b) Hydraulic head measured at JEME moulin (blue), and moulin head corrected for atmospheric pressure variability shown in a, (navy dashed line).

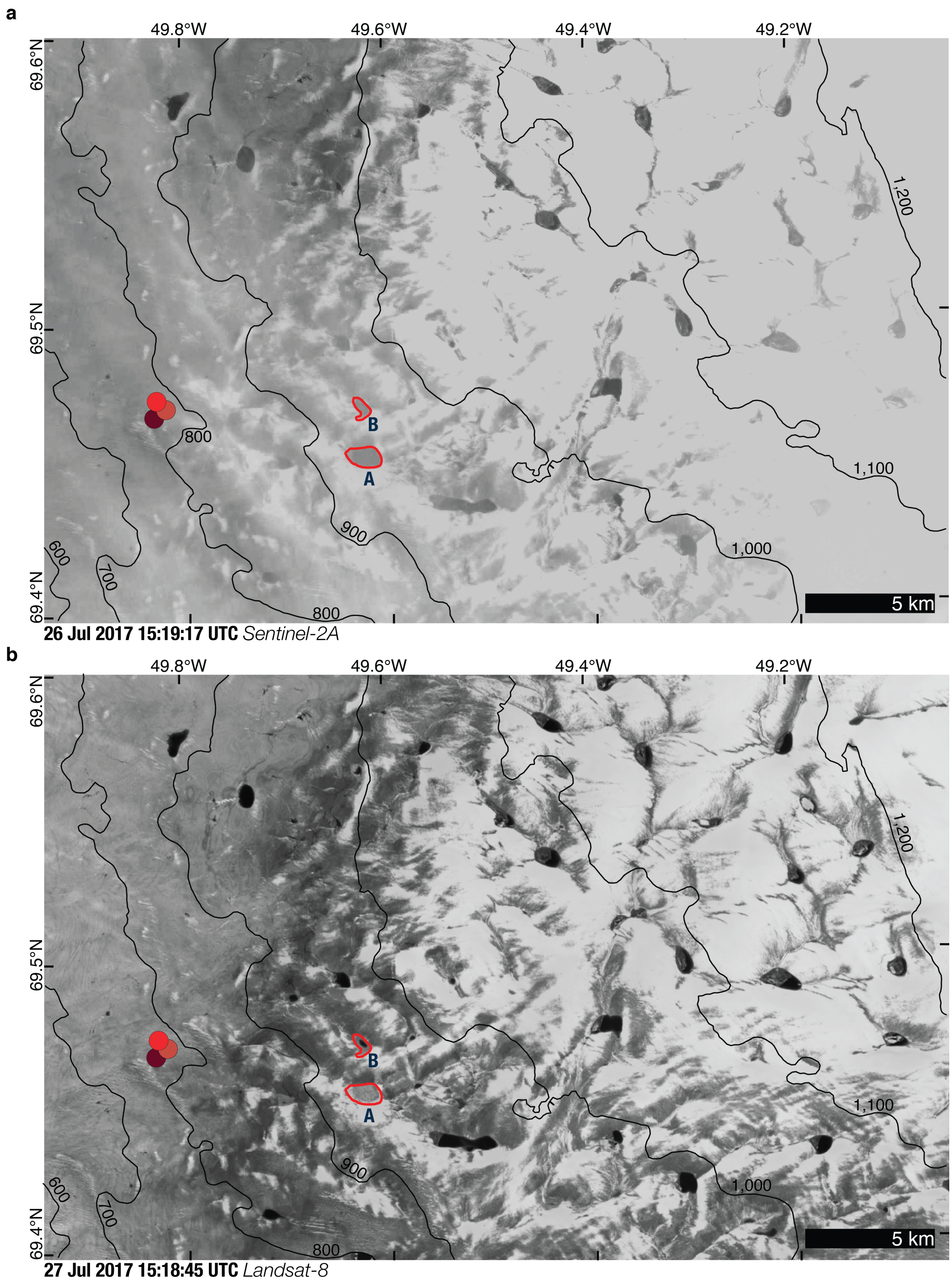

Figure S6. Satellite imagery constraints on 2017 lake drainages. a, Sentinel-2A image from 26 July 2017 at 15:18:17 UTC showing the maximum extents of supraglacial lakes A and B (red), with the location of our instruments (red circles). b, Landsat-8 image acquired on 27 July 2017 at 15:18:45 UTC showing the drainage of lakes A and B, maximum extents same as in a. Surface elevation contours (m) are from BedMachine-v3.

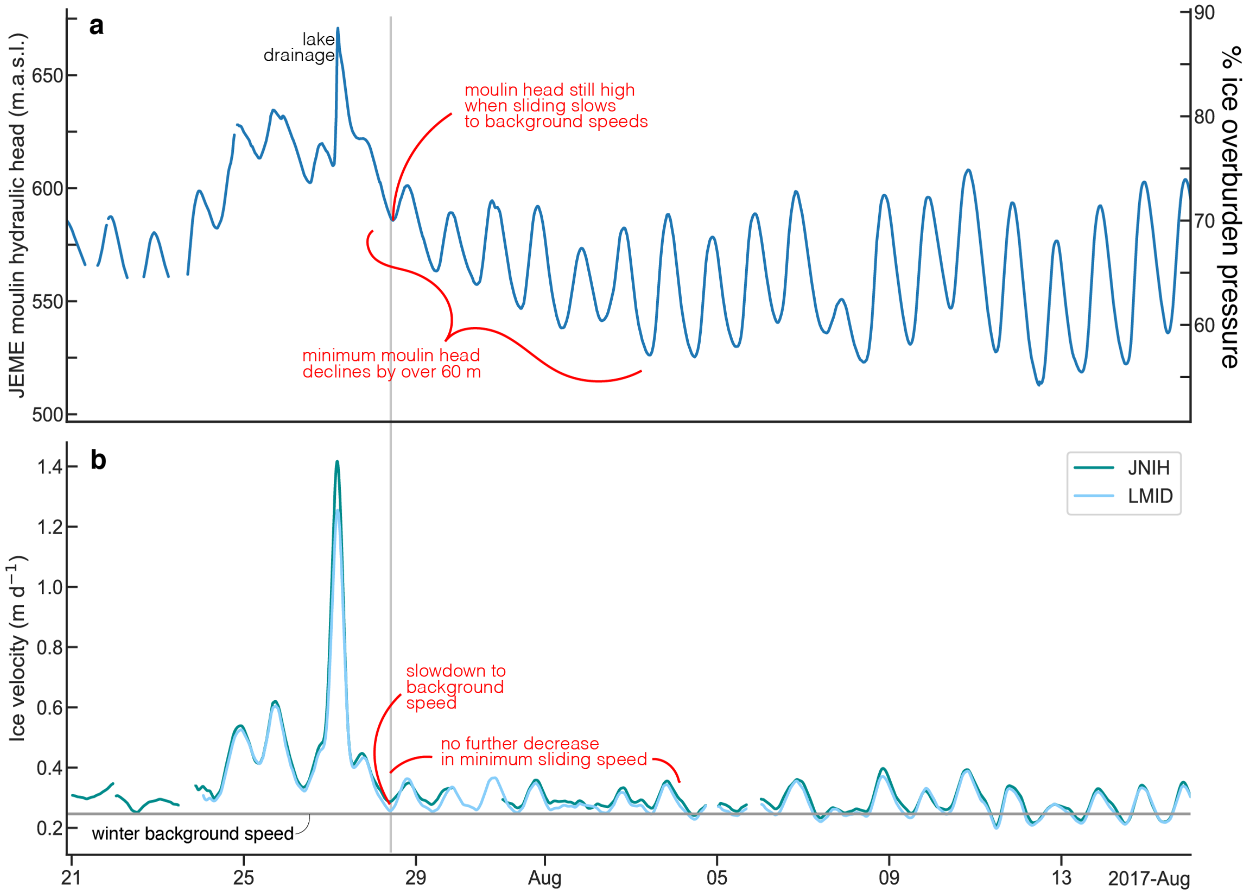

Figure S7. Moulin head and ice velocity timeseries showing 2017 lake drainage event. a, JEME moulin hydraulic head (located in the same position as PIRA which formed in its place during early 2018). b, Along-flow ice velocity from stations LMID (light blue) and JNIH (teal). This timeseries is interrupted by the passing of subglacial floodwaters on 28 July 2017. Sliding slows to winter background speeds (gray) despite high moulin head. Diurnal minimum moulin head falls over the subsequent week, amounting to 60 m (same magnitude as the lake drainage increase) but there is no further decrease in ice velocity as would be expected if increased channelization controlled minimum sliding speed.